

Fast and Incremental Loop Closure Detection with Deep Features and Proximity Graphs

Shan An, *Member, IEEE*, Haogang Zhu, *Member, IEEE*, Dong Wei,
and Konstantinos A. Tsintotas, *Member, IEEE*

Abstract—In recent years, methods concerning the place recognition task have been extensively examined from the robotics community within the scope of simultaneous localization and mapping applications. In this article, an appearance-based loop closure detection pipeline is proposed, entitled “FILD++” (Fast and Incremental Loop closure Detection). When the incoming camera observation arrives, global and local visual features are extracted through two passes of a single convolutional neural network. Subsequently, a modified hierarchical-navigable small-world graph incrementally generates a visual database that represents the robot’s traversed path based on the global features. Given the query sensor measurement, similar locations from the trajectory are retrieved using these representations, while an image-to-image pairing is further evaluated thanks to the spatial information provided by the local features. Exhaustive experiments on several publicly-available datasets exhibit the system’s high performance and low execution time compared to other contemporary state-of-the-art pipelines.

Index Terms—visual-based navigation, mapping, loop closure detection, recognition, convolutional neural networks, hierarchical navigable small-world graph indexing

I. INTRODUCTION

AUTONOMOUS robots have to be capable of exploring unknown areas while at the same time a reliable map of the environment is constructed [1], [2]; the reason is the appropriate representation of the surroundings aiming to be utilized for their localization during navigation. This process is widely known as Simultaneous Localization and Mapping (SLAM) and constitutes an essential component for any modern system [3]. Within the SLAM context, place recognition, i.e., the ability to recognize previously visited locations, plays a primary role in the generation of a valid map [4]. In recent years, the improved computational power of mobile robotic platforms allowed cameras to be adopted as the main perception unit to record the appearance of the scene [5]–[8]. Hence, the utilization of range and bearing sensors, such as laser scanners, radars or sonars, in place recognition tasks

Shan An and Haogang Zhu are with the School of Computer Science and Engineering, Beihang University, Beijing, 100191, China, e-mail: haogangzhu@buaa.edu.cn.

Wei Dong is with Tech & Data Center, JD.COM Inc.

Konstantinos A. Tsintotas is with the Department of Production and Management Engineering, Democritus University of Thrace, Xanthi 67132, Greece, e-mail: ktsintot@pme.duth.gr

Manuscript received June, 2020

© 2020 IEEE. Personal use of this material is permitted. Permission from IEEE must be obtained for all other uses, in any current or future media, including reprinting/republishing this material for advertising or promotional purposes, creating new collective works, for resale or redistribution to servers or lists, or reuse of any copyrighted component of this work in other works.

can be avoided [9]–[11]. Throughout the agent’s mission, the noisy sensor measurements, modeling inaccuracies, and errors due to field abnormalities affect the map construction. The identification of known locations in the traversed route based on the incoming camera information, aiming to rectify the incremental pose drift, is noted as visual loop closure detection [12]–[15]. This operation is, to a great extent, highly related to image retrieval since the system tries to find the most similar visual entry into an already captured database viz., pre-visited camera observations. Two main stages, namely *filtering* and *re-ranking* represent its procedure [16]. Regarding *filtering*, the images in database are ranked in accordance with their similarity to the query, i.e., the current robot’s view. Then, during *re-ranking* each candidate image-pair, originated from *filtering*, is verified depending on the spatial correspondences of their visual data [17].

Early studies in image retrieval task used global description vectors, such as color or texture, to represent the camera measurements [18]–[20]. The frameworks which followed moved towards the utilization of local information, extracted through point-of-interest detection and description methods [21]–[24], to find the most similar candidates into the database. These methods provided robust detection against rotation and scale changes. However, both description types tend to exhibit weakness in cases where intense lighting variations are presented. Furthermore, their extraction process constitutes the bottleneck for any image retrieval system, whilst this is aggravated when local features are preferred since a large amount of description elements is extracted especially in highly textured environments [25]. These drawbacks led the research community to adopt more sophisticated solutions, e.g., the quantization of the descriptor space, indenting to produce a lower amount of meaningful information and faster indexing. The new data is then referred to as visual vocabulary and consists of a specific quantity of visual words.

The so-called Bag-of-Words (BoW) scheme [26], usually constructed through k -means clustering [27], employs the widely used Term-Frequency Inverse-Document-Frequency (TF-IDF) technique to generate visual words histograms that represent the incoming sensory measurements. Through histogram comparisons, the proper image-pair is indicated in many BoW-based place recognition approaches [28]–[32]. High performances are provided in such approaches, while low execution times are achieved due to the utilization of several indexing techniques viz., hierarchical k -means tree [33], k -d tree [34], k -NN graph [35], inverted multi-index file system [36]. Nevertheless, their functionality is highly dependent on

the training environment wherein the visual data is extracted and, in turn, the produced vocabulary. In order to cope with such dependencies, some frameworks related to the visual loop closure detection task incorporate mechanisms to generate the vocabulary in an incremental fashion during the agent's mission [37]–[41]. However, due to the nature of their database construction, these pipelines mostly utilize voting techniques to highlight the candidate locations.

In recent years, Convolutional Neural Network (CNN)-based features tend to replace the traditional handcrafted extraction methods [42]–[46]. Their high performance and outstanding discrimination power demonstrated in tasks such as image classification [47] and scene recognition [48], inspired the research community to use specific network layers as image descriptors. Afterward, the proper image is retrieved following comparison techniques, similar to BoW-schemes ones, over the extracted description vectors [49]. However, as aforementioned, the topological information included in camera measurements –crucial for data association between image-pairs within SLAM– is missing in the case of location's global representation. Yet, in later works, local CNN-based features are extracted from particular image segments. The pioneer algorithm regarding this process is DEep Local Feature (DELF) [50]. Key-points are selected owing to an attention mechanism, while the description stage is achieved using dense localized features. Finally, Principal Component Analysis (PCA) -whitening reduces the descriptor space improving the accuracy during retrieval, whilst maintains the overall memory consumption low as well [51].

In this work, we are interested in the generation of an incremental database, i.e., the map, which permits a fast and scalable detection of loop closures using the provided visual information. Deep features are extracted from each incoming image through a CNN and a modified Hierarchical Navigable Small World (HNSW) graph [52] is built during navigation mapping this way the robot's traversed path. Thus, a faster nearest neighbor (NN) search than contemporary incremental methods is achieved, offering extremely low computational indexing. A preliminary version of this framework was presented in [46]. This article extends this pipeline by improving its performance through the addition of local visual information, extracted via two forward passes of a single network, beyond the global one. This way, we manage to select robustly the appropriate image since we exploit the locations' spatial information through a geometrical verification step which is based on the calculation of a valid fundamental matrix between the chosen pair [53]. The presented algorithm is evaluated experimentally against a total of eleven benchmark datasets. As a final note, the source code¹ of our Fast and Incremental Loop closure Detection (FILD) pipeline, dubbed as "FILD++", is made publicly available to academia indenting to facilitate future studies.

The remainder of this paper is organized as follows: in Section II, a literature review of the most remarkable pipelines regarding the visual loop closure detection is provided. The Section III describes the utilized deep features and Section

IV introduces our HNSW graph database. In Section V, the proposed detection pipeline is presented in detail, while the experimental protocol along with the comparative results follow in Sections VI and VII. Finally, Section VIII discusses the proposed approach and concludes providing our future plans.

II. RELATED WORK

Appearance-based loop closure detection is a widely attracting task in the robotics community. This section presents a literature review regarding the approaches which tackle it. Aiming to provide a better path for the reader's understanding, we categorize these studies according to their main feature-extraction tool, namely hand-crafted and CNN-based ones.

A. Approaches using Hand-crafted Features

To cope with the large amount of extracted features, many scholars quantized the visual elements in order to generate a visual vocabulary. According to the database construction process, these studies are distinguished into off-line and on-line ones. Concerning the off-line approaches, Fast Appearance-Based MAPping (FAB-MAP) [5] introduced the visual vocabulary model aiming to mitigate the quantity of the extracted SURF points-of-interest [22], while a Chow Liu tree was adopted to learn the co-visibility between these words [55]. The same authors proposed an enhanced version of this system that handled large-scale environments [6]. The BoW model proposed in [28] was built based on binary local features. Using geometrical verification checks, this framework avoided the false-positive detections. Later, an improved version of the same pipeline [29] utilized ORB features [24] to incorporate rotation and scale invariance properties. Similarly, loops were detected and corrected inside the Parallel Tracking and Mapping (PTAM) framework [56]. Groups-of-images were represented by a common visual words histogram in [30], while group matching is performed coherently advancing along with time [31].

While the aforementioned approaches relied on a static visual vocabulary, which is adapted to the training environment, in [38] an on-line and incrementally constructed database was proposed to identify loops through the matching probability of a Bayesian scheme. In a similar manner, an agglomerative clustering algorithm was adopted to generate the method's visual vocabulary [33]. The stability between visual elements' associations was attained using an incremental image-indexing process in conjunction with a tree-based feature-labeling method. The Real-Time Appearance-Based Mapping (RTAB-Map) framework [39] proposed a memory management mechanism in order to utilize a limited number of candidate locations. An Incremental bag of BIrary words for Appearance based Loop closure Detection (IBuILD) was formulated in [40]. Visual words were generated through feature matching between consecutive images, while a likelihood function decided about the chosen image-pair. Hierarchical Topological Mapping (HTMap) presented a loop closure scheme based on the Pyramid Histogram of Oriented Gradients (PHOG) [57] global description vectors for

¹<https://github.com/AnshanTJU/FILD>

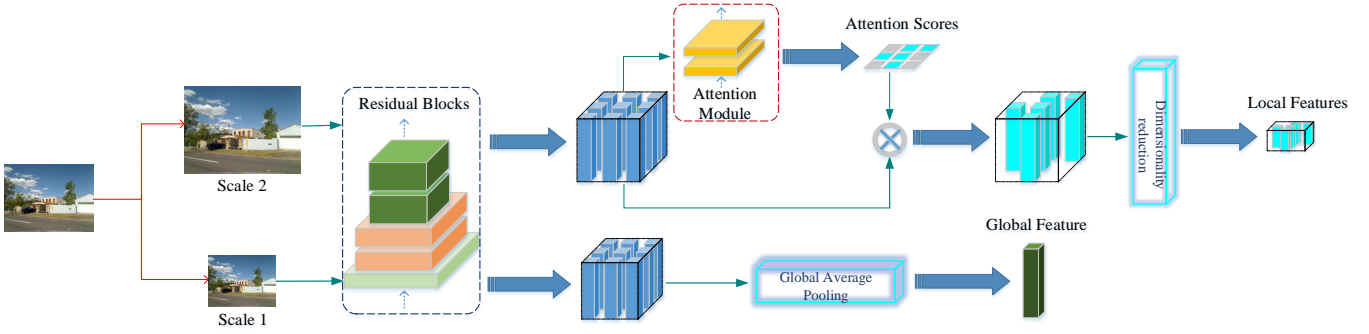


Fig. 1. The architecture of our feature-extractor module. A fully convolutional network generate specific representations from the incoming imagery using a modified version of DELF [50]. Global and local deep features are produced through two passes of the network. The network consists of three components: the backbone network which is based on the residual blocks of ResNet50 [54], the global and the local feature extraction branches. As the original image enters to the system is resized to different scales before proceeds to the network. The features extracted from the first scale are feeded into a global average pooling technique for global representations' production, while features from the second scale are sent into the local branch. An attention module is adopted for the corresponding scores' generation, while the more relevant are assigned with higher scores. Finally, we select the appropriate features and using a dimension reduction method to extract the final local local representations.

image representation [58]. Similar locations were highlighted due to binary local features correspondences. An incremental approach that utilized binary descriptors and dynamic islands was proposed by iBoW-LCD [59]. Similarly, in [41], the incoming image stream was dynamically segmented formulating places that were represented by unique visual words. A probabilistic voting scheme followed, aiming to indicate the proper place, while an image-to-image pairing was held based on the locations' local features correspondences. An incremental vocabulary constructed through local features tracking was presented in [8]. Comparisons were performed using locations' probabilistic score derived from a binomial density function [60].

B. Approaches using Convolutional Neural Networks Features

The impressive performance of CNNs, exhibited on a wide variety of tasks, was the main reason to become the principal tool for many modern systems that address the visual place recognition task. Utilizing an end-to-end trainable architecture, NetVLAD was proposed for similar locations' identification [61]. This network proposed a trainable, via backpropagation, generalized VLAD layer, which can be plugged into any CNN architecture. Later, a Spatial Pyramid-Enhanced VLAD (SPE-VLAD) layer was built encoding feature extraction and improving loss function [62]. PCANet employed a cascaded deep network to extract unsupervised features, which were subsequently used as image descriptors improving the accuracy of a loop closure detection pipeline [63]. Investigating the internal structure of networks, CNN-based features were extracted in [64] through the detection and representation of salient regions directly from the convolutional layer activations. Cascianelli et al. proposed a visual scene modeling technique that preserved the geometric and semantic structure and, at the same time, improved the appearance invariance [65]. Condition- and viewpoint-invariant features were generated when a multi-scale pooling was employed in [66]. In [67], an Omnidirectional CNN (O-SCC) was proposed aiming

to mitigate the challenge of severe camera pose variations. The authors in [68] proposed an attention mechanism capable of being incorporated into an existing feed-forward network architecture in order to learn image representations for long-term place recognition applications. An effective similarity measurement for the detection of pre-visited locations in changing environments was proposed in [69]. Combining a neural network inspired by the Drosophila olfactory neural circuit (FlyNet) and a 1-d Continuous Attractor Neural Network (CANN), a compact system with high performances was proposed by [70]. These works commonly use CNNs to extract the global descriptor of a whole scene, while only a few methods employ CNNs to extract local information. In this article, two types of features, global and local ones, are extracted aiming to better represent an image using a single network.

III. IMAGE REPRESENTATION

Our feature-extractor relies on a Fully Convolutional Network (FCN), which we aim to use in order to generate specific representations from the incoming imagery. A modified version of DELF extracts both global and local deep features in different scales through two passes of the network, in contrast to the original method. We choose as the backbone of the proposed network the initial three convolutional blocks of ResNet50 [54], while the output of the last layer is provided as input to our features' extraction sub-modules, as depicted in Fig. 1.

A. Global Features

A Global Average Pooling (GAP) [71] layer is applied to the feature map space $w \times h \times c$, generated by the FCN, aiming to produce a single description vector for the incoming visual information. Here, w , h , c are the width, height, and the channels of the feature map. As a result, the feature map is reduced to a dimensionality of $1 \times 1 \times c$ since the GAP layer produces a single number per channel, which is the average of all values $w \times h$.

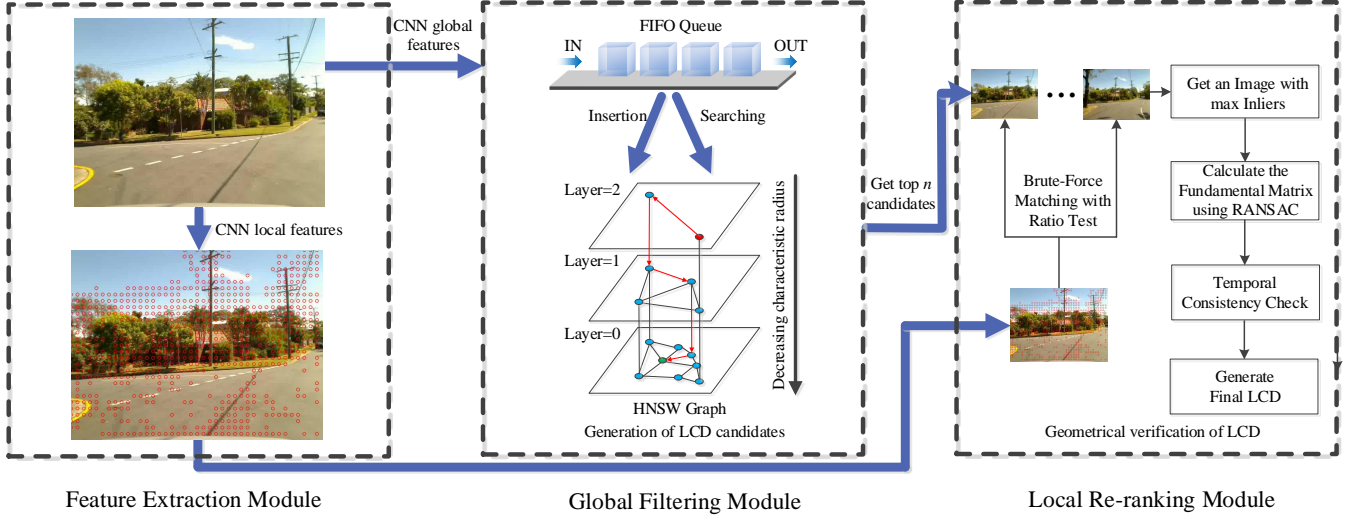


Fig. 2. An overview of the proposed loop closure detection pipeline. Global and local Convolution Neural Network (CNN)-based features are extracted as the incoming image stream enters the system. The first ones enter the First-In-First-Out (FIFO) queue, and subsequently, they insert into the Hierarchical Navigable Small World (HNSW) graph [52] in order to generate the incremental database. Using the same procedure, the top n nearest neighbors are indicated at query time, while a brute force matching technique between the candidate image-pairs is performed at local features space. A ratio test is implemented to eliminate false matches in conjunction with a RANSAC-based geometrical verification check. Finally, a temporal consistency check is employed to approve the final loop closure pair.

B. Attention-based Local Features

We consider each pixel of the feature map as a local grid. This yields the dense sample representation of the feature map. The tensor composed through all grid channels is treated as a local feature, while the corresponding keypoint is located to the center of the receptive field in the pixel coordinates. An attention module, whose purpose is to learn a score function for each feature, follows, composed of two CNN layers of 1×1 convolutional filters. A subset of the extracted features is selected based on the satisfaction of a score threshold δ since many of the extracted elements have negative effects. In the second layer, a softplus activation [72] is deployed to ensure the score is non-negative. A score map is generated with a size of $w \times h \times 1$ corresponding to every local feature and keypoint. This local feature extraction process is totally different from the traditional hand-crafted methods, such as SIFT [21] or SURF [22], which firstly detect keypoints and subsequently they describe them.

C. Local Features' Dimensionality Reduction

Aiming to reduce the description space, we follow the commonly used method of [51]. Our extracted local features are subjected to L_2 normalization before the utilization of the PCA technique. The generated 40-bin dimensionality space is also processed through L_2 normalization.

D. Features' Scales

To extract representative and robust features, we propose to use different scales during the extraction process. In contrast to the DELF [50] method, where image pyramids are constructed using seven different scales, we chose to use as global descriptor the first scale and the second one for the

local features' extraction. We propose these two scales since the pyramid generation is a computationally costly process and our aim is to build a system with low complexity and high performance. As a result, the incoming sensory data is resized based on the aforementioned scales before it is applied as input to our network.

IV. HIERARCHICAL NAVIGABLE SMALL WORLD GRAPH DATABASE

Our system employs the HNSW graph to index the generated global deep features. The proposed method is selected since it constitutes a reliable technique which outperforms other modern search methods [52], such as tree-based BoW [73], product quantization NN [74] and locality sensitive hashing [75]. The following sub-sections present the proposed technique, our database construction, as well as the modified search process oriented for the loop closure detection task.

A. Hierarchical Navigable Small World

A graph $G = (V, E)$ consists of a set of nodes V and a set of links E between them. The HNSW, originated from the Navigable Small World (NSW) model [76], constitutes a graph based on an incremental k -NN structure, as shown in Fig. 2. A link e_{ab} directly connects the nodes a and b , which in our case are represented by the extracted global description vectors. As node's neighborhood is defined the set of its immediately connected elements, while as its degree the size of this set. The preferred indexing technique is chosen against its ancestor since it can alleviate the major drawback presented in other proximity graphs and related to its performance degradation when confronting low dimensional or clustered data [52]. In the NSW scheme, both the average number of hops and nodes' degree on a single greedy search

scale polylogarithmic [77]. On the other hand, the proposed model uses different strategies in order to select specific nodes, separate links from different scales, and chose neighbors using an advanced heuristic. According to the links' length into different layers a robust separation is achieved. Then, the search process is performed in a hierarchical multilayer graph allowing logarithmic scalability.

B. Database Construction and Exploration

In contrast to BoW-based approaches, where the visual vocabulary is generated during a training stage, the proposed pipeline constructs its database during the robot's navigation, eliminating the usage of any previous data. An integer maximum layer l is randomly selected with an exponentially decaying probability distribution for every inserted element q . Traversing the graph from the higher layer to the lower i.e., the ground, the ef closest neighbors in each layer are indicated as the enter nodes to the next one. This lasts until the M connections of the inserted element reach the ground level, while the normalized scalar product (cosine of the angle between vectors) is selected as distance metric between the corresponding global features:

$$s_{pq} = \frac{X_p^T \cdot X_q}{\|X_p\|_2 \cdot \|X_q\|_2}. \quad (1)$$

s_{pq} is the distance score between images I_p , I_q , and X_p , X_q are the global description vectors. $\|X\|_2 = \sqrt{X^T X}$ denotes the L_2 norm of vector X . Finally, since we aim to build a low computational system, we make use of the Advanced Vector Extensions [78] instructions to accelerate the pipeline.

V. DETECTION PIPELINE

A. System Overview

As the robotic platform navigates into the working area, its incoming sensory information, provided by the mounted camera, passes through the CNN in order the global and local features to be extracted. The global features are used for the HNSW graph's generation and the retrieval task, while the local ones are utilized for the geometrical verification. Temporal consistency checks follow to protect the system from possible false-positive detections. An overview of the proposed scheme is illustrated in Fig. 2, while its steps are given in Algorithm 1.

B. Non-Search Area Definition

Since the incoming images are captured sequentially, the adjacent to query ones are highly possible to share semantic information yielding to high similarities between them. When querying the database, this area, i.e., images acquired close in time, have to be rejected from the searching process because false-positive detections will occur. Therefore, we design a First-In-First-Out (FIFO) queue to store our global visual representations. As shown in Algorithm 1, the deep feature X_i , belonging to Image I_i , firstly enters the queue Q , and subsequently, it remains there aiming to be inserted into the HNSW graph when the robot runs out of the non-search area.

Algorithm 1 Our Loop Closure Detection Algorithm

Input: the image I_i captured by the visual sensory module during robot's navigation; the excluded area, defined by frame N_{non} as $\psi \times \phi$, where ψ is a temporal constant and ϕ is the frame rate of the camera; the returned number of nearest neighbors n ; the threshold of inlier points τ .
Output: whether the i detection constitute a loop or not.

```

1: initialize a FIFO queue  $Q$ .
2: while true do  $\triangleright$  perform the loop closure detection pipeline
   during agent's mission.
3:    $I_i \leftarrow$  read the current image
4:    $X_i, L_i \leftarrow$  extract deep global feature  $X_i$  and deep
   local features  $L_i$  of this image.
5:   if ( $i > N_{non}$ ) then
6:      $X_{pre} \leftarrow$  pop the FIFO queue  $Q$ .
7:     add  $X_{pre}$  to HNSW graph database.
8:      $k$ -nearest neighbor search of  $X_i$  in the database to
   obtain the  $n$  nearest neighbors.
9:      $inlier_{max} \leftarrow -1$ ,  $ind \leftarrow -1$ 
10:    for  $r = 1$  to  $n$  do
11:      perform geometrical verification for  $L_i$  and  $L_r$ 
12:      if failed then
13:        continue
14:      end if
15:       $inlier \leftarrow$  the number of inliers
16:      if  $inlier > inlier_{max}$  then
17:         $inlier_{max} \leftarrow inlier$ 
18:         $ind \leftarrow r$ 
19:      end if
20:    end for
21:    temporal consistency check for  $L_i$  and  $L_{ind}$ 
22:    if success then
23:      Loop detected.
24:    end if
25:  end if
26:  push  $X_i$  to the FIFO queue  $Q$ .
27: end while

```

This area is defined based on a temporal constant ψ , and the camera's frame rate ϕ . Consequently, when we use the current feature as query, it will only search in database area defined via $N - \psi \times \phi$, where N is the number of the entire set of camera measurements up to time i . As a final note, the images in the non-search area will never appear in the results.

C. Image Matching

At query time, a similar procedure as in Section IV is performed. The main difference is that the closest neighbors from the ground layer are returned in the results, while the search quality is controlled by the parameter ef . As described in Section III, we extract the local deep features for each incoming image and the matching process is performed between the query q and the n closest neighbors based on a brute-force matching algorithm. Even though, many state-of-the-art methods which make use of pre-trained vocabularies, adopt FLANN [83] method for indexing aiming to avoid the high

TABLE I
DESCRIPTIONS OF THE USED DATASETS

Dataset		Description	Image Resolution	# Images	Frame rate (Hz)	Distance (km)
KITTI [79]	Seq# 00	Outdoor, dynamic	1241 × 376	4541	10	3.7
	Seq# 02		1241 × 376	4661		5.0
	Seq# 05		1226 × 370	2761		2.2
	Seq# 06		1226 × 370	1101		1.2
Oxford	New College [80]	Outdoor, dynamic	512 × 384	52480	20	2.2
	City Center [5]		640 × 480	1237		1.9
Malaga 2009 [81]	Parking 6L	Outdoor, slightly dynamic	1024 × 768	3474	7	1.2
St. Lucia [82]	100909 (12:10)	Outdoor, dynamic	640 × 480	19251	15	~17.6
	100909 (14:10)			20894		
	180809 (15:45)			21434		
	190809 (08:45)			21815		

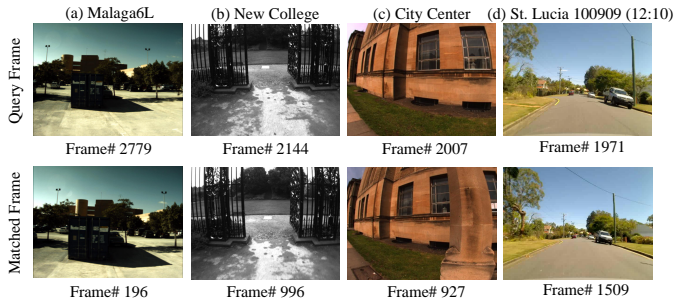


Fig. 3. Some image pairs which are not labelled as loops in the ground truth derived from GPS logs.

complexity of the greedy search, we prefer the latter case since our feature-extractor generates low dimensionality (40-bins) description vectors in contrast to the traditional techniques viz., SIFT (128-bins) and SURF (64-bins or 128-bins). A distance ratio check [21] is employed on the proposed pair defined through a threshold ε .

D. Geometrical Verification

Our system incorporates a geometrical verification step to discard outliers, i.e., false-positive detections. In order to achieve this we try to compute the fundamental matrix T between the chosen candidate pair of images using a RANSAC-based scheme. If the calculation succeeds, we record the candidate with the highest number of inliers.

E. Temporal Consistency Check

As the final step, a temporal consistency check is employed intending to examine whether the aforementioned conditions are met for β consecutive camera measurements [41]. This way, the proposed pipeline may lose a possible loop closing identification in cases where the query image is the initial in a sequence of pre-visited locations, however we prefer to prevent the system from wrong identifications preserving a perfect precision score. When the aforementioned conditions are met, the matched pair is recognized as a loop closure event.

VI. EXPERIMENTAL PROTOCOL

A. Benchmark Datasets

Eleven challenging and publicly available image-sequences are chosen in order to evaluate the performance of our loop closure detection framework. These datasets are captured in different operating environments viz., various lighting conditions, strong visual repetition, and dynamic occlusions such as cars and pedestrians. The detailed description of each used dataset is listed in Table I. In KITTI vision suite [79], Malaga 2009 Parking 6L (Malaga6L) [81] and St. Lucia [82], the incoming input stream obtained by a camera mounted on a moving car, while the New College [80] and City Center [5] are recorded through the vision system of a wheeled robot. Since the Malaga6L, New College, and City Center are composed of stereo images, we chose the left camera stream for the first one and the right camera measurements for the rest. Our experimental setup is chosen aiming to coincide the settings adapted in [49]. For the New College and St. Lucia image-sequences, frame rate is selected at 1 Hz and 3 Hz respectively to reduce the overlap between the frames, whilst the other datasets are processed according to their frame rate.

B. Existing Problems

Commonly, the ground truth data referring to the correct loop closures candidates are generated according to GPS logs. For example, the ground truth matrices for St. Lucia and Malaga6L in [49] are derived through the utilization of GPS distance-range of 10 meters and 4 meters, respectively, from the query. We carefully checked these data for each of the eleven datasets recognizing that some image pairs are not labeled correctly, as shown in Fig. 3. In many cases, this happens because the robot traverses to positions that surpass the GPS's distance threshold, although the captured visual contents are similar. However, in such cases, if the fundamental matrix can be computed, then a transformation matrix between the two camera poses is provided, indicating a true detection that has to be recognized from the SLAM system. Therefore, these pairs should be treated as a correct loop event. Another problem concerns the situation where the robot is exactly in the same place, but the camera points to



Fig. 4. A labeling correction: the image sequence in first row shows the robot's trajectory as it turns to the right road, while in the second row it turns to the left road at the same place. Frames #835 and #147 are visually different, but are labelled as loops according to the GPS for its distance lower than 10 meters. During our experiments these images are considered as true-negative pairs.

a different angle resulting to visually different images; hence, the image pairs are not same and should not be considered as a loop in a place recognition system, as shown in Fig. 4.

1) *Manually Labelling*: Considering that the GPS logs are not accurate, we preferred to generate human-labeled ground truth matrices. The produced pairs are chosen to locations shorter than a distance metric range of 40 meters as it is preferred than most methods in the related section. During labeling, if a decision was hard to be taken, the proposed pairs are re-checked by experts familiar with the place recognition task. Each of the aforementioned datasets is processed two times before used, while for the KITTI image-sequences, the data were accurate enough avoiding this procedure. Our accurate, manually-labeled ground truth files would be made publicly available in order to facilitate further studies.

VII. EXPERIMENTAL RESULTS

The following section presents the experiments conducted to demonstrate the effectiveness of the proposed framework. Experimental settings including training strategies, parameters, and evaluation metrics are introduced in VII-A, while different settings for the proposed feature extraction module are evaluated and compared against the traditional extraction methods in VII-B. Subsequently, we analyze the HNSW parameterization followed by the efficiency evaluation of our local re-ranking module. The system's performance is discussed in VII-E, whilst a quantitative comparison with the state-of-the-art is presented in VII-G. Finally, we measure the computational cost and memory footprint of our system in VII-F.

A. Experimental Settings

1) *Training Strategies*: Since our feature extraction module is hard to get trained directly because of the attention module usage, a two-step strategy is applied. Firstly, our base network is trained without the attention module and subsequently two fully connected layers are added for classification. ResNet50, which constitutes our base, is trained on the ImageNet [84], and then is fine-tuned on a large-scale landmark dataset [85].

When our training process is over, its weights are squeezed and the attention module is added. The resulted score map is used to pool the features through a weighted sum before they enter to the fully connected layer for the classification using the cross entropy loss. This model is utilized in order to obtain the discriminative visual deep features.

2) *Training Parameters*: Aiming to train the base network, we use the SGD optimizer with an initial learning rate of 0.001, with 25 epochs as maximum number of training while during every 10 epochs the learning rate decays to half of the previous. Similarly, for the attention module, the SGD optimizer was selected with an initial learning rate to be set at 0.01, at maximum number of 20 epochs and learning rate which decays to half of the previous every 10 epochs. We implement the two networks using the batch size of 256.

3) *Baseline approaches*: The compared approaches include classic and recently proposed loop closure detection systems consisting of the DLoopDetector [28], Tsintotas et al. [41], PREVIEW [31], iBoW-LCD [59], Kazmi et al. [49], as well as our previous method FILD [46]. Most of the compared methods are implemented using their open source codes provided by the corresponding authors. For Kazmi's method, we directly report their results as published in their article.

4) *Evaluation Metrics*: For the loop closure detection task, the commonly used metric is the recall rate at 100% precision. The precision-recall metric is defined as:

$$Precision = \frac{tp}{tp + fp} \quad (2)$$

$$Recall = \frac{tp}{tp + fn} \quad (3)$$

where tp is the number of true positives, indicating the detected loop closures are true loops according to the ground truth. fp is the number of false positives, representing the identifications found by the algorithm; however, these are not labeled to ground truth. fn is the number of false negatives, indicating the number of true loops not found by the algorithm.

5) *Implementation*: The experiments were performed on a Linux machine with an Intel Xeon CPU E5-2640 v3 (2.60GHz) CPU and an Nvidia P40 GPU. More specifically,

TABLE II
THE RECALL AT 100% PRECISION AND THE FEATURE EXTRACTION SPEED (MS) ON DIFFERENT SCALES OF GLOBAL AND LOCAL FEATURES

Scales (Global)	Scales (Local)													
	0.25		0.35		0.5		0.7		1.0		1.4		2.0	
	recall	speed	recall	speed	recall	speed	recall	speed	recall	speed	recall	speed	recall	speed
0.25	0.9123	8.11	0.9073	8.90	0.9010	10.01	0.9123	12.54	0.9135	16.49	0.9261	28.25	0.9236	56.07
0.35	0.8972	8.73	0.9273	9.40	0.9110	10.56	0.9110	13.19	0.8960	17.14	0.8960	28.86	0.9023	56.28
0.5	0.8972	9.61	0.9110	10.28	0.9098	11.23	0.9261	14.00	0.9110	17.93	0.9492	29.62	0.9480	57.15
0.7	0.8972	11.73	0.9110	12.41	0.8997	13.56	0.9248	16.09	0.9098	19.90	0.9492	31.79	0.9492	59.01
1.0	0.8910	14.61	0.8985	15.25	0.8935	16.22	0.9261	18.77	0.9035	22.64	0.9211	34.53	0.9323	61.90
1.4	0.8922	20.95	0.9035	21.69	0.8935	22.47	0.9286	24.96	0.9048	28.89	0.9223	40.26	0.9336	68.97
2.0	0.8947	35.08	0.9023	35.57	0.8960	36.46	0.9261	38.95	0.9060	42.76	0.9223	53.97	0.9336	81.00

TABLE III
PARAMETER LIST

Image scale for global feature extraction s_g	0.5
Image scale for local feature extraction s_l	1.4
Score threshold of local feature δ	15
Number of nearest to q elements to return, ef	40
Maximum number of connections for each element per layer, M	48
Search area time constant, ψ	40
Ratio of ratio test, ε	0.7
Images temporal consistency, β	2
Number of of matches for geometrical verification, n	5

only the feature extraction was performed on the GPU; other operations all use the CPU. The proposed network is implemented via TensorFlow framework, but bindings are provided for the feature extraction module as well as other parts of our algorithm in C++. For timing recording, we also implement our algorithm on an NVIDIA Jetson TX2 GPU and reported the measurements in subsection VII-F.

B. Evaluation on Image Scales

The original DELF approach utilizes image pyramids to generate descriptors of different scales. These scales range from 0.25 to 2.0, which are a $\sqrt{2}$ factor apart. Since for the mobile robot application the processing time is crucial in our framework we propose to use one scale for the global extraction and another one for the local extraction. We conduct extensive experiments to evaluate the recall rate and the extraction speed through different scales. In Table II, the results of different combinations are presented for KITTI 00 image-sequence, while the scales which achieve the highest 3 recall rates are marked in blue. As shown, the scales of 0.7 and 2.0 for global and local deep features, respectively, reach the highest recall value at 100% precision, whilst a similar score can be achieved at scales of 0.5 and 0.7 for global features, and 1.4 for local. Considering the extraction time, we choose the scales of 0.5 and 1.4, which get the same recall via a computational time below 30 ms. It is also notable that for scales of 0.25 for both global and local deep features, the extraction time is only 8.11 ms. The parameters of our algorithm are summarized in Table III, which are determined according to the experiments in Section VII-B, VII-C, VII-D.

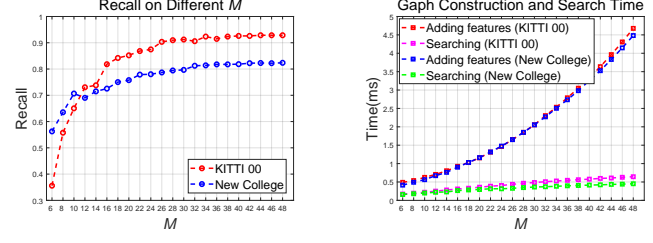


Fig. 5. (Left) The recall at 100% precision of our algorithm on the KITTI 00 dataset [79] and the New College dataset [80] using a different M from 6 to 48. (Right) The time for adding feature to the graph and the searching time on the KITTI 00 dataset and the New College dataset using a different M .

C. Evaluation on HNSW Parameters

For HNSW graph construction, two parameters exists that affect the search quality. More specifically, the total ef of NN to q and the maximum number of connections for each element per layer, M . The range of the parameter ef should be within 300, because an increase in the value of ef leads to a better performance, however its construction time is significantly longer. The range of the parameter M should be 5 to 48 [52]. The experiments in [52] showed that a bigger M is better for high recall and high dimensional data, which also defines the memory consumption of the algorithm.

We perform the experiments on the KITTI 00 and New College datasets in order to choose the proper M and ef values. During M selection, the parameter ef was set to 40, while the number n of matches for geometrical verification was set to 5. The precision-recall curves are shown in the left part of Fig. 5. It is observed that when M increases, the recall score follows. In the right part of Fig. 5, feature addition and search time are increased when M increases. To achieve a better recall, we choose $M = 48$ in the following experiments.

The evaluation of ef is presented in the left part of Fig. 6. As shown, the recall scores do not significantly change when this parameter increases. In the right part of Fig. 6, the feature addition time increases as ef does, while the searching time remains stable. Therefore, we choose $ef = 20$ for our method.

D. Evaluation on Geometrical Verification

Because the computational time for matching and RANSAC are relatively high, we only evaluate parameters from $n = 1$ to $n = 10$ in the experiments. As shown in Fig. 7, the time for

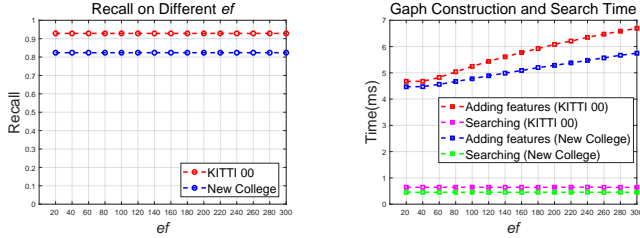


Fig. 6. (Left) The recall at 100% precision of our algorithm on the KITTI 00 dataset [79] and the New College dataset [80] using a different ef from 20 to 300. (Right) The time for adding feature to the graph and the searching time on the KITTI 00 dataset and the New College dataset using a different ef .

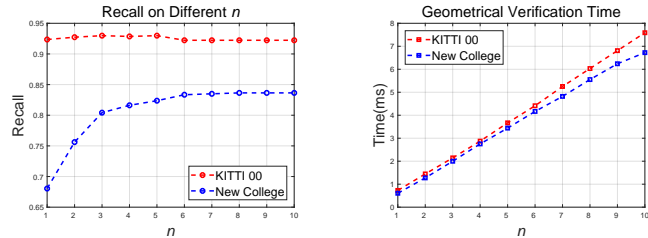


Fig. 7. (Left) The recall at 100% precision of our algorithm on the KITTI 00 dataset [79] and the New College dataset [80] using a different number of matches n for geometrical verification. (Right) The time for geometrical verification on the KITTI 00 dataset and the New College dataset using a different n .

geometrical verification increases linearly while n increases. For the KITTI 00 environment, time varies from 0.73 ms to 7.59 ms for $n = 1$ to $n = 10$, respectively, while the recall at 100% precision holds about the same score. In the case of New College, the timing fluctuates from 0.61 ms to 6.72 ms for $n = 1$ to $n = 10$, however a better recall is achieved when its value increases. To balance the recall and the processing time, we choose as parameter $n = 5$.

We also evaluate the processing time for different image matching strategies: the FLANN method [83] and the Brute-Force matcher. For the KITTI 00 dataset, the average time of the Brute-Force matcher is 3.32 ms, while FLANN costs 40.70 ms, on average, whilst for New College, the times are 0.91 ms and 15.62 ms, respectively. As shown in Fig. 8, we can see that the matching time using the Brute-Force

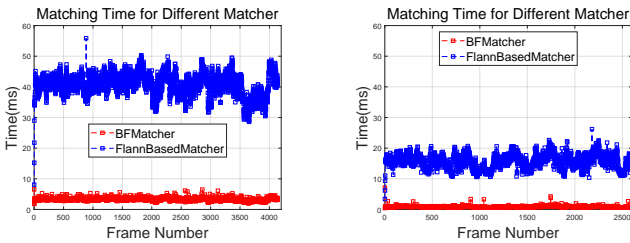


Fig. 8. The image matching time of our algorithm on the KITTI 00 dataset [79] (Left) and the New College dataset [80] (Right) using different matching strategies.

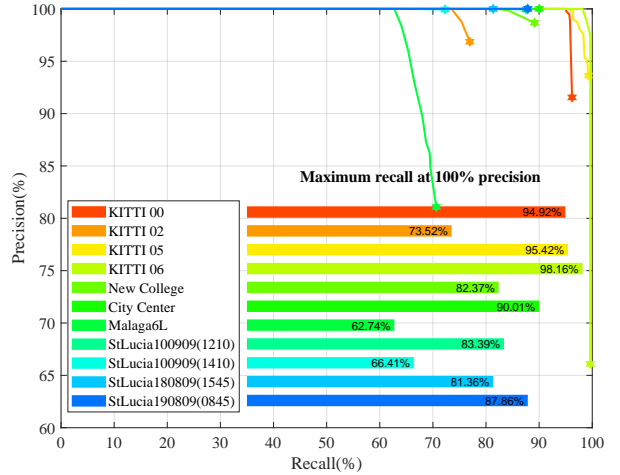


Fig. 9. The precision-recall curve of our algorithm on eleven datasets.

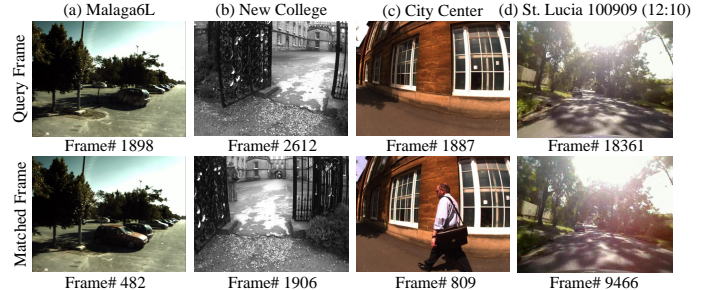


Fig. 10. Some example images of the detected loop-closure locations.

matcher is significantly lower than FLANN, because of the low dimension (40-bins) of our local feature.

E. The performance of Our Framework

We evaluate the performance of our loop closure detection framework on eleven commonly used datasets, presented in Table I. Fig. 9 shows the precision-recall curves generated by varying the inlier number. The proposed method can successfully detect the loop closure from 62.74% (for Malaga6L) to 98.16% (for KITTI 06) of the times. The Malaga6L is the most challenging dataset among these eleven datasets, because the frames are captured on repetitive and very close roads. The KITTI 06 is the smallest one among the rest, where our pipeline achieves the highest recall of 98.16%.

Some examples of detected loop-closure matches are shown in Fig. 10. For the dynamic objects in environment, cars in Fig. 10a and a person in Fig. 10c, the algorithm can detect the correct match. The example in Fig. 10b demonstrate that our algorithm can handle the viewpoint change, while Fig. 10d shows the ability of our algorithm to deal with the lighting change. The loop closures detected by our framework for the robot's trajectories are illustrated in Fig. 11.

F. Time Requirements

We calculate the computational cost of our algorithm on four representative datasets. The times for feature extraction

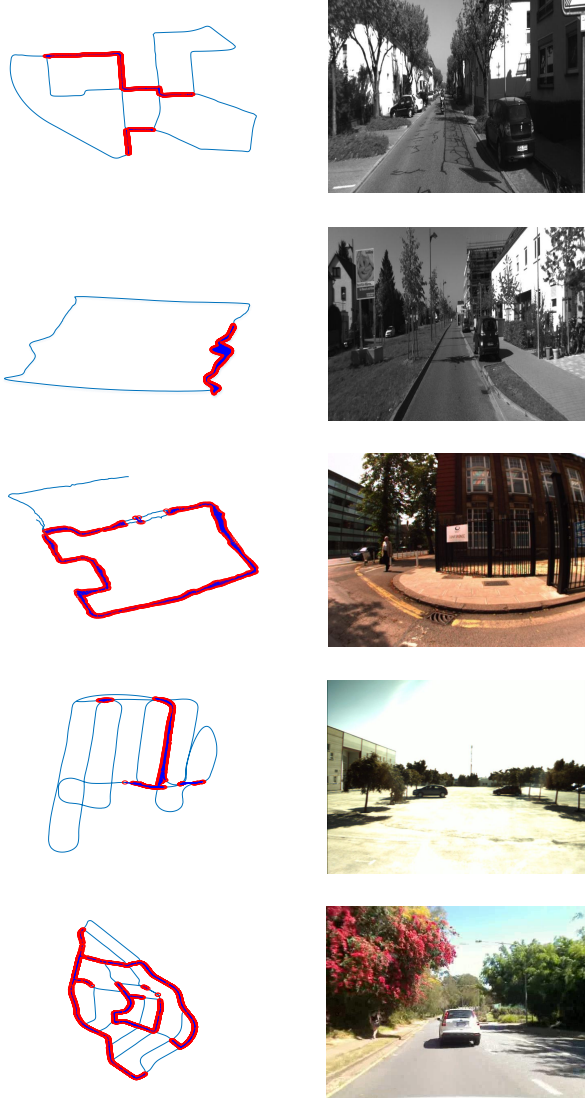


Fig. 11. Robot trajectories (left) and example images (right). From top to bottom: KITTI 00 [79], KITTI 06 [79], City Center [5], Malaga6L [81], St. Lucia 100909 (12:10) [82]. The loop closure detections are labelled using red circles.

and loop detection are recorded as a function of the frame number, as shown in Fig. 12. Our algorithm requires nearly constant time for all the datasets, which not increases accordingly to the frame's number. For the Malaga6L image-sequence, the proposed method requires about 50 to 80 ms for the total execution time. This happens since the image resolution is the largest of these evaluated datasets, while for the St. Lucia timings are below 40 ms because of the image's resolution.

The times for different stages of our algorithm are shown in Table IV. It is observed that the feature extraction stage is the most costly stage. For the Malaga6L dataset, the feature extraction requires about 45 ms, making it the slowest among them. We can see that our indexing graph technique is below 1 ms and that the speed of the whole system ranges from 32 ms to 57 ms demonstrating the high efficiency of our algorithm.

In order to test the scalability of the system, we set the

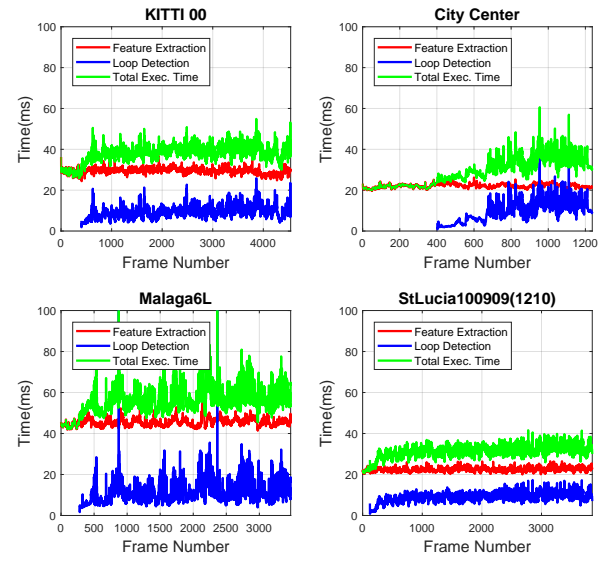


Fig. 12. Execution time of our algorithm. Note the loop detection starts after $\psi \times \phi$ frames.

TABLE IV
EXECUTION TIME (MS/QUERY) OF OUR METHOD IN DIFFERENT DATASETS

Stages	KITTI 00	City Center	Malaga6L	St. Lucia 100909 (12:10)
Feature Extraction	29.67	22.04	45.41	22.48
Adding Feature	4.69	4.30	3.63	6.03
Graph Searching	0.64	0.33	0.47	0.70
Feature Matching	3.32	2.17	4.13	2.26
RANSAC	0.38	3.26	2.92	2.73
Whole System	38.70	32.10	56.56	34.20

frequency to $f = 20\text{Hz}$ and obtained 52480 images. The execution time consumed per image in that case is shown in Table V. The average running time per image was about 22 ms. It can be seen in Fig. 13, the increase of the frames will not bring increased time for processing.

We also implement our algorithm on the Jetson TX2 platform in Max-N mode (all CPU cores in use and GPU clocked at 1.3 GHz). The execution time is shown in Fig. 14. Our algorithm does not require more time for processing a frame

TABLE V
EXECUTION TIME (MS/QUERY) IN NEW COLLEGE DATASET WITH 52480 IMAGES

Stages	Mean	Std	Max	Min
Feature Extraction	14.62	0.65	21.13	12.30
Adding Feature	3.97	2.47	22.63	0.04
Graph Searching	0.67	0.19	3.20	0.04
Feature Matching	1.06	0.10	14.04	0.08
RANSAC	1.72	1.08	17.01	0.0
Whole System	22.05	5.04	58.98	14.56

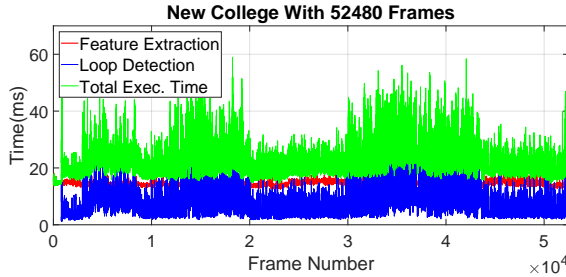


Fig. 13. Execution time in New College dataset with 52480 images. Note the loop detection starts after $\psi \times \phi$ frames.

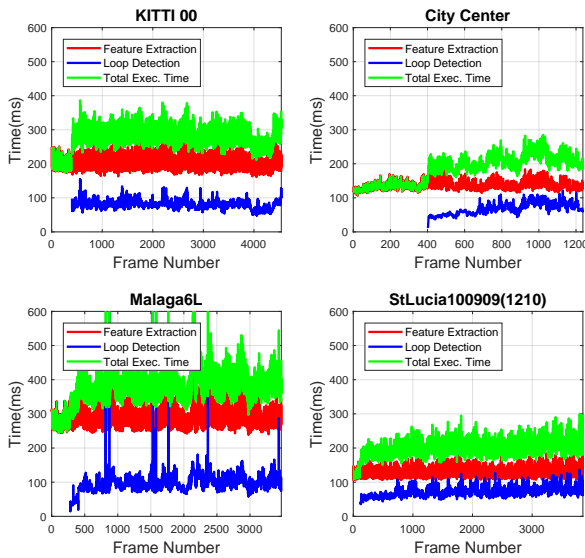


Fig. 14. Execution time on an NVIDIA Jetson TX2 GPU. Note the loop detection starts after $\psi \times \phi$ frames.

even in an embedded platform. The most time-consuming module is the feature extraction because we perform two forward passes on two images with scales of 0.5 and 1.4. In Table VI, we list the average time for the feature extraction, the loop detection, and the whole system. For the Malaga6L dataset, the average time for the whole system is 388.66 ms. For other datasets, the average processing times are below 300 ms meaning that our algorithm is fast on embedded systems.

G. Comparison with the Baseline Techniques

In Table VII, we list the highest recall of our algorithm at 100% precision on eleven datasets compared to the baseline methods. Our method outperforms the baseline methods on all the datasets except the KITTI 02 dataset, and two St. Lucia datasets.

The image sequences of the Malaga6L dataset are captured at the parking of the Computer Science Faculty of the University of Malaga (Spain). There is no distinct difference between the roads, and there are many trees, which causes an extremely high scene similarity. Therefore, every method works poorly in this dataset. Our method outperforms others,

TABLE VI
EXECUTION TIME (MS/QUERY) ON AN NVIDIA JETSON TX2 GPU

Stages	KITTI 00	City Center	Malaga6L	St. Lucia 100909 (1210)
Feature Extraction	200.12	135.97	292.06	128.19
Loop Detection	78.84	68.44	96.60	72.39
Whole System	278.96	204.41	388.66	200.58

particularly in KITTI and in Oxford datasets. This is because there are relatively more architectures in these datasets, which are similar to the training set of our feature extraction network. Our method can extract more representative features and compare them better for these scenes.

We compare the average execution time of different methods on four datasets. As shown in Table VIII, the FILD++ method performs faster than the previous method FILD. This improvement is because of our deep local features' low dimension and the corresponding high speed image matching. The processing speeds of these methods are highly related to the size of the input image. For example, almost all the methods get slowest processing time on the Malaga6L dataset, for its image size of 1024×768 , which is bigger than others.

VIII. DISCUSSION AND CONCLUSION

In this article, a fast and incremental loop closure detection approach is proposed, which is dubbed as FILD++. Our pipeline extracts global and local deep features for filtering and re-ranking, respectively, through two forward passes of a single network. Along the robot's navigation, an HNSW graph is built incrementally based on global features permitting the fast indexing as well as the fast database search for similar pre-visited locations during query. Finally, the selected pair is geometrically verified via the provided local deep features. Eleven publicly available datasets are used for our experiments, presenting the effectiveness and efficiency of the proposed system compared against other contemporary state-of-the-art pipelines.

Our system's performance depends on several factors: the performance of the deep global and local features, the retrieval precision of the HNSW graphs, and the effectiveness of the geometrical verification. We did not utilize the similarity scores of the query and the returned images. A proper threshold may have helped us eliminate false positives. However, the complexity of the system will be increased inevitably. In the geometrical verification step, the number of matches n is an important parameter. The easiest way is the increase of n to achieve a higher recall. As illustrated before, the increase of n will cost more time for the geometrical verification. Therefore, a balance needs to be considered.

For our future plans, we intend to integrate the proposed method to a SLAM framework. Moreover, an increase in the classification accuracy will lead to an increase of recall in the whole system, therefore using more powerful networks, such as ResNeXt [86] and ResNeSt [87], will naturally improve the performance of our system.

TABLE VII
RECALLS AT 100% PRECISION: A COMPARISON OF THE BASELINE METHODS WITH OUR FRAMEWORK

Dataset	DLoopDetector [28] [†]	Tsintotas et al. [41]	PREVIEW [31] [‡]	iBoW-LCD [59] [§]	Kazmi et al. [49] [¶]	FILD [46]	FILD++
KITTI	Seq# 00	72.43	93.18	89.47	76.50	90.39	91.23
	Seq# 02	68.22	76.01	71.96	72.22	79.49	65.11
	Seq# 05	51.97	94.20	87.71	53.07	81.41	85.15
	Seq# 06	89.71	86.03	80.15	95.53	97.39	98.16
Oxford	New College	47.56	52.44	80.87	73.14	51.09	76.74
	City Center	30.59	16.30	49.63	82.03	75.58	66.48
Malaga 2009	Parking 6L	31.02	59.14	33.93	57.48	50.98	56.09
St. Lucia	100909 (12:10)	37.22	26.27	60.93	70.02	80.06	76.06
	100909 (14:10)	14.87	9.77	23.06	68.06	58.10	53.84
	180809 (15:45)	31.36	15.07	49.79	87.50	72.55	66.96
	190809 (08:45)	39.78	27.68	56.69	59.36	80.13	78.00

[†] We use different number of images for New College and Malaga6L datasets compared to [28]. We change the normalized similarity score threshold to achieve 100% precision, because there are false detections using the default parameters. [‡] We report the recall using the default parameters. However, the precision of each dataset cannot achieve 100%. [§] We report the iBoW-LCD recalls on KITTI dataset from [49]. [¶] We directly report the results in [49], because the author did not provide the implementation.

TABLE VIII
AVERAGE EXECUTION TIME (MS/QUERY) ON THE REPRESENTATIVE DATASETS

Approach	KITTI 00	City Center	Malaga6L	St. Lucia 100909 (1210)
DLoopDetector [28]	111.04	27.51	42.57	91.04
Tsintotas et al. [41]	521.54	183.23	638.61	625.05
PREVIEW [31]	32.39	34.09	36.33	25.40
FILD [46]	62.68	40.23	68.16	49.10
FILD++	38.70	32.10	56.56	34.20

ACKNOWLEDGMENT

The authors wish to gratefully acknowledge Dr. Mark Cummins for his kindly help, as well as Guangfu Che and Fangru Zhou, whose constructive suggestions helped the system evaluation.

REFERENCES

- [1] E. Garcia-Fidalgo and A. Ortiz, “Vision-based topological mapping and localization methods: A survey,” *Robotics and Autonomous Systems*, vol. 64, pp. 1–20, 2015.
- [2] I. Kostavelis and A. Gasteratos, “Semantic mapping for mobile robotics tasks: A survey,” *Robotics and Autonomous Systems*, vol. 66, pp. 86–103, 2015.
- [3] C. Cadena, L. Carlone, H. Carrillo, Y. Latif, D. Scaramuzza, J. Neira, I. Reid, and J. J. Leonard, “Past, present, and future of simultaneous localization and mapping: Toward the robust-perception age,” *IEEE Trans. Robot.*, vol. 32, no. 6, pp. 1309–1332, Dec 2016.
- [4] S. Lowry, N. Snderhauf, P. Newman, J. J. Leonard, D. Cox, P. Corke, and M. J. Milford, “Visual place recognition: A survey,” *IEEE Trans. Robot.*, vol. 32, no. 1, pp. 1–19, Feb. 2016.
- [5] M. Cummins and P. Newman, “FAB-MAP: Probabilistic localization and mapping in the space of appearance,” *Int. J. Robot. Res.*, vol. 27, no. 6, pp. 647–665, Jun. 2008.
- [6] ———, “Appearance-only SLAM at large scale with FAB-MAP 2.0,” *Int. J. Robot. Res.*, vol. 30, no. 9, pp. 1100–1123, Nov. 2011.
- [7] J. Engel, J. St̄ckler, and D. Cremers, “Large-scale direct slam with stereo cameras,” in *IEEE/RSJ Int. Conf. Intell. Robots Syst.*, Oct. 2015, pp. 1935–1942.
- [8] K. A. Tsintotas, L. Bampis, and A. Gasteratos, “Probabilistic appearance-based place recognition through bag of tracked words,” *IEEE Robot. Autom. Lett.*, vol. 4, no. 2, pp. 1737–1744, Apr. 2019.
- [9] J.-S. Gutmann and K. Konolige, “Incremental mapping of large cyclic environments,” in *IEEE Int. Symp. Comp. Intell. Robot. Autom.*, Nov. 1999, pp. 318–325.
- [10] M. G. Dissanayake, P. Newman, S. Clark, H. F. Durrant-Whyte, and M. Csorba, “A solution to the simultaneous localization and map building (slam) problem,” *IEEE Trans. Robot. Autom.*, vol. 17, no. 3, pp. 229–241, Jun. 2001.
- [11] J. D. Tard̄os, J. Neira, P. M. Newman, and J. J. Leonard, “Robust mapping and localization in indoor environments using sonar data,” *Int. J. Robot. Res.*, vol. 21, no. 4, pp. 311–330, Apr. 2002.
- [12] K. L. Ho and P. Newman, “Loop closure detection in SLAM by combining visual and spatial appearance,” *Robot. Auton. Syst.*, vol. 54, no. 9, pp. 740 – 749, Sep. 2006.
- [13] C. Mei, G. Sibley, and P. Newman, “Closing loops without places,” in *IEEE/RSJ Int. Conf. Intell. Robots Syst.*, Oct. 2010, pp. 3738–3744.
- [14] H. Zhang, “BORF: Loop-closure detection with scale invariant visual features,” in *IEEE Int. Conf. Robot. Autom.*, May 2011, pp. 3125–3130.
- [15] K. A. Tsintotas, L. Bampis, and A. Gasteratos, “DOSeqSLAM: Dynamic on-line sequence based loop closure detection algorithm for SLAM,” in *IEEE Int. Conf. Imag. Sys. Techn.*, Oct. 2018, pp. 1–6.
- [16] M. Teichmann, A. Araujo, M. Zhu, and J. Sim, “Detect-to-retrieve: Efficient regional aggregation for image search,” in *IEEE Conf. Comp. Vis. Pattern Recogn.*, Jun. 2019, pp. 5109–5118.
- [17] F. Radenovic, A. Iscen, G. Tolias, Y. Avrithis, and O. Chum, “Revisiting oxford and paris: Large-scale image retrieval benchmarking,” in *IEEE Conf. Comp. Vis. Pattern Recogn.*, Jun. 2018, pp. 5706–5715.
- [18] A. Oliva and A. Torralba, “Modeling the shape of the scene: A holistic representation of the spatial envelope,” *Int. J. of Comp. Vis.*, vol. 42, no. 3, pp. 145–175, 2001.
- [19] A. Torralba, K. P. Murphy, W. T. Freeman, M. A. Rubin *et al.*, “Context-based vision system for place and object recognition,” in *IEEE Conf. Comp. Vis.*, vol. 3, 2003, pp. 273–280.
- [20] A. Oliva and A. Torralba, “Building the gist of a scene: The role of global image features in recognition,” *Progr. Brain Res.*, vol. 155, pp. 23–36, 2006.
- [21] D. G. Lowe, “Distinctive image features from scale-invariant keypoints,” *Int. J. of Comp. Vis.*, vol. 60, no. 2, pp. 91–110, Nov. 2004.
- [22] H. Bay, T. Tuytelaars, and L. Van Gool, “Surf: Speeded up robust features,” in *Euro. Conf. Comp. Vis.*, May 2006, pp. 404–417.
- [23] M. Calonder, V. Lepetit, C. Strecha, and P. Fua, “Brief: Binary robust independent elementary features,” in *Euro. Conf. Comp. Vis.*, Sep. 2010, pp. 778–792.
- [24] E. Rublee, V. Rabaud, K. Konolige, and G. Bradski, “Orb: An efficient alternative to sift or surf,” in *IEEE Conf. Comp. Vis.*, Nov. 2011, pp. 2564–2571.
- [25] K. A. Tsintotas, P. Giannis, L. Bampis, and A. Gasteratos, “Appearance-based loop closure detection with scale-restrictive visual features,” in *Proc. Int. Conf. Comput. Vis. Syst.*, Nov. 2019, pp. 75–87.
- [26] J. Sivic and A. Zisserman, “Video google: A text retrieval approach to object matching in videos,” in *IEEE Conf. Comp. Vis.*, Oct. 2003, p. 1470.

[27] J. MacQueen *et al.*, “Some methods for classification and analysis of multivariate observations,” in *roc. Berkeley Symp. Math. Statist. Prob.*, vol. 1, no. 14, 1967, pp. 281–297.

[28] D. Gálvez-López and J. D. Tards, “Bags of binary words for fast place recognition in image sequences,” *IEEE Trans. Robot.*, vol. 28, no. 5, pp. 1188–1197, Oct. 2012.

[29] R. Mur-Artal and J. D. Tards, “Fast relocation and loop closing in keyframe-based SLAM,” in *IEEE Int. Conf. Robot. Autom.*, May 2014, pp. 846–853.

[30] L. Bampis, A. Amanatiadis, and A. Gasteratos, “Encoding the description of image sequences: A two-layered pipeline for loop closure detection,” in *IEEE/RSJ Int. Conf. Intell. Robots Syst.*, Oct. 2016, pp. 4530–4536.

[31] ———, “Fast loop-closure detection using visual-word-vectors from image sequences,” *Int. J. Robot. Res.*, vol. 37, no. 1, pp. 62–82, Dec. 2018.

[32] K. A. Tsintotas, L. Bampis, S. Rallis, and A. Gasteratos, “SeqSLAM with bag of visual words for appearance based loop closure detection,” in *Proc. Int. Conf. Robot. in Alpe-Adria Danube Region.*, Jun. 2018, pp. 580–587.

[33] T. Nicosevici and R. Garcia, “Automatic visual bag-of-words for online robot navigation and mapping,” *IEEE Trans. Robot.*, vol. 28, no. 4, pp. 886–898, Aug. 2012.

[34] Y. Liu and H. Zhang, “Indexing visual features: Real-time loop closure detection using a tree structure,” in *IEEE Int. Conf. Robot. Autom.*, 2012, pp. 3613–3618.

[35] K. Hajebi and H. Zhang, “An efficient index for visual search in appearance-based slam,” in *IEEE Int. Conf. Robot. Autom.* IEEE, 2014, pp. 353–358.

[36] A. Babenko and V. Lempitsky, “The inverted multi-index,” *IEEE Trans. Pattern Analys. Mach. Intell.*, vol. 37, no. 6, pp. 1247–1260, 2014.

[37] D. Filliat, “A visual bag of words method for interactive qualitative localization and mapping,” in *IEEE Int. Conf. Robot. Autom.*, 2007, pp. 3921–3926.

[38] A. Angeli, D. Filliat, S. Doncieux, and J. Meyer, “Fast and incremental method for loop-closure detection using bags of visual words,” *IEEE Trans. Robot.*, vol. 24, no. 5, pp. 1027–1037, Oct. 2008.

[39] M. Labb and F. Michaud, “Appearance-based loop closure detection for online large-scale and long-term operation,” *IEEE Trans. Robot.*, vol. 29, no. 3, pp. 734–745, Jun. 2013.

[40] S. Khan and D. Wollherr, “IBuILD: Incremental bag of binary words for appearance based loop closure detection,” in *IEEE Int. Conf. Robot. Autom.*, May 2015, pp. 5441–5447.

[41] K. A. Tsintotas, L. Bampis, and A. Gasteratos, “Assigning visual words to places for loop closure detection,” in *IEEE Int. Conf. Robot. Autom.*, May 2018, pp. 5979–5985.

[42] A. Babenko, A. Slesarev, A. Chigorin, and V. Lempitsky, “Neural codes for image retrieval,” in *Euro. Conf. Comp. Vis.* Springer, Sep. 2014, pp. 584–599.

[43] N. Sünderhauf, S. Shirazi, F. Dayoub, B. Upcroft, and M. Milford, “On the performance of convnet features for place recognition,” in *IEEE/RSJ Int. Conf. Intell. Robots Syst.*, 2015, pp. 4297–4304.

[44] Y. Hou, H. Zhang, and S. Zhou, “Convolutional neural network-based image representation for visual loop closure detection,” in *IEEE Int. Conf. Infor. Autom.*, 2015, pp. 2238–2245.

[45] A. Gordo, J. Almazán, J. Revaud, and D. Larlus, “Deep image retrieval: Learning global representations for image search,” in *Euro. Conf. Comp. Vis.* Springer, Oct. 2016, pp. 241–257.

[46] S. An, G. Che, F. Zhou, X. L. Liu, X. Ma, and Y. Chen, “Fast and incremental loop closure detection using proximity graphs,” in *IEEE/RSJ Int. Conf. Intell. Robots Syst.*, Nov. 2019, pp. 378–385.

[47] A. Krizhevsky, I. Sutskever, and G. E. Hinton, “Imagenet classification with deep convolutional neural networks,” in *Adv. Neural Inf. Process. Syst.*, Dec. 2012, pp. 1097–1105.

[48] B. Zhou, A. Lapedriza, J. Xiao, A. Torralba, and A. Oliva, “Learning deep features for scene recognition using places database,” in *Adv. Neural Inf. Process. Syst.*, Dec. 2014, pp. 487–495.

[49] S. A. M. Kazmi and B. Mertsching, “Detecting the expectancy of a place using nearby context for appearance-based mapping,” *IEEE Trans. Robot.*, vol. 35, no. 6, pp. 1352–1366, 2019.

[50] H. Noh, A. Araujo, J. Sim, T. Weyand, and B. Han, “Large-scale image retrieval with attentive deep local features,” in *IEEE Conf. Comp. Vis.*, Oct. 2017, pp. 3456–3465.

[51] H. Jegou and O. Chum, “Negative evidences and co-occurrences in image retrieval: The benefit of pca and whitening,” in *Euro. Conf. Comp. Vis.*, 2012, pp. 774–787.

[52] Y. A. Malkov and D. A. Yashunin, “Efficient and robust approximate nearest neighbor search using hierarchical navigable small world graphs,” *IEEE Trans. Pattern Analysis and Machine Intell.*, Dec. 2018.

[53] M. A. Fischler and R. C. Bolles, “Random sample consensus: a paradigm for model fitting with applications to image analysis and automated cartography,” *Communications of the ACM*, vol. 24, no. 6, pp. 381–395, 1981.

[54] K. He, X. Zhang, S. Ren, and J. Sun, “Deep residual learning for image recognition,” pp. 770–778, Jun. 2016.

[55] C. Chow and C. Liu, “Approximating discrete probability distributions with dependence trees,” *IEEE Trans. Infor. Theory*, vol. 14, no. 3, pp. 462–467, May 1968.

[56] G. Klein and D. Murray, “Parallel tracking and mapping for small ar workspaces,” in *IEEE and ACM Int. Symp. Mixed. Aug. Real.*, Nov. 2007, pp. 225–234.

[57] A. Bosch, A. Zisserman, and X. Munoz, “Representing shape with a spatial pyramid kernel,” in *Proc. ACM Int. Conf. Image and Video Retrieval*. ACM, Jul. 2007, pp. 401–408.

[58] E. Garcia-Fidalgo and A. Ortiz, “Hierarchical place recognition for topological mapping,” *IEEE Trans. Robot.*, vol. 33, no. 5, pp. 1061–1074, Jun. 2017.

[59] ———, “iBoW-LCD: An appearance-based loop-closure detection approach using incremental bags of binary words,” *IEEE Robot. Autom. Lett.*, vol. 3, no. 4, pp. 3051–3057, 2018.

[60] M. Gehrig, E. Stumm, T. Hinzmann, and R. Siegwart, “Visual place recognition with probabilistic voting,” in *IEEE Int. Conf. Robot. Autom.*, May 2017, pp. 3192–3199.

[61] R. Arandjelovic, P. Gronat, A. Torii, T. Pajdla, and J. Sivic, “Netvlad: Cnn architecture for weakly supervised place recognition,” in *IEEE Conf. Comp. Vis. Pattern Recogn.*, June. 2016, pp. 5297–5307.

[62] J. Yu, C. Zhu, J. Zhang, Q. Huang, and D. Tao, “Spatial pyramid-enhanced netvlad with weighted triplet loss for place recognition,” *IEEE Trans. Neur. Net. and Learn. Syst.*, vol. 31, no. 2, pp. 661–674, Feb. 2020.

[63] Y. Xia, J. Li, L. Qi, and H. Fan, “Loop closure detection for visual slam using pcanet features,” in *IEEE Joint Conf. Neur. Net.*, Jul. 2016, pp. 2274–2281.

[64] Z. Chen, F. Maffra, I. Sa, and M. Chli, “Only look once, mining distinctive landmarks from convnet for visual place recognition,” in *IEEE/RSJ Int. Conf. Intell. Robots Syst.*, Sep. 2017, pp. 9–16.

[65] S. Cascianelli, G. Costante, E. Bellocchio, P. Valigi, M. L. Fravolini, and T. A. Ciarfuglia, “Robust visual semi-semantic loop closure detection by a covisibility graph and cnn features,” *Robotics and Autonomous Systems*, vol. 92, pp. 53–65, Jun. 2017.

[66] Z. Chen, A. Jacobson, N. Sünderhauf, B. Upcroft, L. Liu, C. Shen, I. Reid, and M. Milford, “Deep learning features at scale for visual place recognition,” in *IEEE Int. Conf. Robot. Autom.*, May 2017, pp. 3223–3230.

[67] T.-H. Wang, H.-J. Huang, J.-T. Lin, C.-W. Hu, K.-H. Zeng, and M. Sun, “Omnidirectional cnn for visual place recognition and navigation,” in *IEEE Int. Conf. Robot. Autom.*, May 2018, pp. 2341–2348.

[68] Z. Chen, L. Liu, I. Sa, Z. Ge, and M. Chli, “Learning context flexible attention model for long-term visual place recognition,” *IEEE Robot. Autom. Lett.*, vol. 3, no. 4, pp. 4015–4022, Oct. 2018.

[69] Z. Xin, X. Cui, J. Zhang, Y. Yang, and Y. Wang, “Real-time visual place recognition based on analyzing distribution of multi-scale cnn landmarks,” *Journal of Intelligent & Robotic Systems*, vol. 94, no. 3-4, pp. 777–792, Jun. 2019.

[70] M. Chancán, L. Hernandez-Nunez, A. Narendra, A. B. Barron, and M. Milford, “A hybrid compact neural architecture for visual place recognition,” *IEEE Robot. Autom. Lett.*, vol. 5, no. 2, pp. 993–1000, Feb. 2020.

[71] M. Lin, Q. Chen, and S. Yan, “Network in network,” *arXiv preprint arXiv:1312.4400*, 2013.

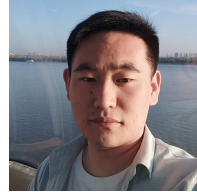
[72] C. Dugas, Y. Bengio, F. Bélisle, C. Nadeau, and R. Garcia, “Incorporating second-order functional knowledge for better option pricing,” in *Adv. Neural Inf. Process. Syst.*, Dec. 2001, pp. 472–478.

[73] M. Muja and D. G. Lowe, “Scalable nearest neighbor algorithms for high dimensional data,” *IEEE Trans. Pattern Analysis and Machine Intell.*, no. 11, pp. 2227–2240, 2014.

[74] H. Jegou, M. Douze, and C. Schmid, “Product quantization for nearest neighbor search,” *IEEE Trans. Pattern Analysis and Machine Intell.*, vol. 33, no. 1, pp. 117–128, 2011.

[75] A. Andoni and I. Razenshteyn, “Optimal data-dependent hashing for approximate near neighbors,” in *Proc. ACM Symp. Theory of computing*, Jun. 2015, pp. 793–801.

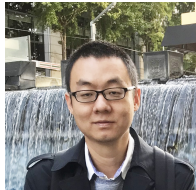
- [76] J. M. Kleinberg, "Navigation in a small world," *Nature*, vol. 406, no. 6798, p. 845, 2000.
- [77] Y. Malkov, A. Ponomarenko, A. Logvinov, and V. Krylov, "Approximate nearest neighbor algorithm based on navigable small world graphs," *Information Systems*, vol. 45, pp. 61–68, Sep. 2014.
- [78] (2011) Introduction to intel advanced vector extensions. [Online]. Available: <https://software.intel.com/en-us/articles/introduction-to-intel-advanced-vector-extensions/>
- [79] A. Geiger, P. Lenz, and R. Urtasun, "Are we ready for autonomous driving? the kitti vision benchmark suite," in *IEEE Conf. Comp. Vis. Pattern Recogn.*, Jun. 2012, pp. 3354–3361.
- [80] M. Smith, I. Baldwin, W. Churchill, R. Paul, and P. Newman, "The new college vision and laser data set," *Int. J. Robot. Res.*, vol. 28, no. 5, pp. 595–599, 2009.
- [81] J.-L. Blanco, F.-A. Moreno, and J. Gonzalez, "A collection of outdoor robotic datasets with centimeter-accuracy ground truth," *Autonomous Robots*, vol. 27, no. 4, p. 327, 2009.
- [82] A. J. Glover, W. P. Maddern, M. J. Milford, and G. F. Wyeth, "Fab-map+ ratslam: Appearance-based slam for multiple times of day," in *IEEE Int. Conf. Robot. Autom.* IEEE, May 2010, pp. 3507–3512.
- [83] M. Muja and D. G. Lowe, "Fast approximate nearest neighbors with automatic algorithm configuration," *Int. Conf. Comp. Vis. Theo. Appl.*, vol. 2, no. 331-340, p. 2, 2009.
- [84] O. Russakovsky, J. Deng, H. Su, J. Krause, S. Satheesh, S. Ma, Z. Huang, A. Karpathy, A. Khosla, M. Bernstein *et al.*, "Imagenet large scale visual recognition challenge," *Int. J. of Comp. Vis.*, vol. 115, no. 3, pp. 211–252, Apr. 2015.
- [85] T. Weyand, A. Araujo, B. Cao, and J. Sim, "Google landmarks dataset v2—a large-scale benchmark for instance-level recognition and retrieval," *arXiv preprint arXiv:2004.01804*, 2020.
- [86] S. Xie, R. Girshick, P. Dollár, Z. Tu, and K. He, "Aggregated residual transformations for deep neural networks," in *IEEE Conf. Comp. Vis. Pattern Recogn.*, Jul. 2017, pp. 1492–1500.
- [87] H. Zhang, C. Wu, Z. Zhang, Y. Zhu, Z. Zhang, H. Lin, Y. Sun, T. He, J. Mueller, R. Mammatha *et al.*, "Resnest: Split-attention networks," *arXiv preprint arXiv:2004.08955*, 2020.



Dong Wei received the Bachelor's degree in mathematics and applied mathematics, and the Master's degree in applied statistics from the Northeastern University, China, in 2017 and 2020, respectively. He is currently an algorithm engineer with Tech & Data Center in JD.COM Inc. His research interests include computer vision in robotics, deep learning and image processing.



Konstantinos A. Tsintotas received the bachelor's degree from the department of automation engineering, Technological Education Institute of Central Greece, Chalkida, Greece and the master's degree in mechatronics from the department of electrical and computer engineering, University of Western Macedonia, Kozani, Greece, in 2010 and 2015, respectively. Since 2016, he has been a Ph.D. candidate in the field of robotic vision at the laboratory of robotics and automation, department of production and management engineering in the Democritus University of Thrace, Xanthi, Greece. His research interests include vision-based place recognition methods for simultaneous localization and mapping applications in mobile, autonomous robots. Details are available at <http://robotics.pme.duth.gr/ktsintotas>.



Shan An received the Bachelor's degree in automation engineering from Tianjin University, China in 2007 and the Master's degree in control science from Shandong University, China, in 2010. He is currently a Ph.D. candidate in the field of computer vision at the School of Computer Science and Engineering in the Beihang University, China. He has serviced as program committee member for ACM Multimedia 2019/2020, ACM Multimedia Asia 2019. He is a reviewer of IEEE Transaction on Neural Network and Learning Systems, IEEE Transaction on Multimedia, Pattern Recognition and Pattern Recognition Letters, etc. His research interests include large scale image retrieval, VSLAM in robotics and AR.



Haogang Zhu received the Ph.D. degree from the University College London, London, United Kingdom. He was Professor of the School of Computer Science and Engineering, Beijing University of Aeronautics and Astronautics from 2015. His main research interest includes Bayesian analysis, machine learning, and image understanding. He worked as the Principle Investigator and Data Scientist on various projects sponsored by research councils and industry leaders such as NIHR UK, Fight for Sight, Heidelberg Engineering, Pfizer, Novartis and Carl Zeiss Meditec. His research has led to several patents and tools/systems used by research institutes and industrial companies. He was awarded a young scientist position in the Chinese Recruitment Program of Global Experts (1000 Talent Plan) in 2015.